14393

Modeling Nanoparticle Formation during Early Stages of Zeolite Growth: A Low-Coordination Lattice Model of Template Penetration

L. Jin,[†] **Scott M. Auerbach,*,**[†,‡] **and P. A. Monson*,**[†]

Department of Chemical Engineering and Department of Chemistry, University of Massachusetts, Amherst, Massachusetts 01003

Received: May 14, 2010; Revised Manuscript Received: July 20, 2010

We present an extension of the simple-cubic lattice model developed by Jorge et al. [*J. Am. Chem. Soc.* **2005**, *127*, 14388] of nanoparticle growth in the clear solution synthesis of silicalite-1 (MFI). We have implemented the model on a body-center cubic (bcc) lattice with second-neighbor repulsions, to generate a four-coordinate network that mimics the tetrahedral structure of silica. With this low-coordination lattice model we observe that the nanoparticles are metastable, possessing a core−shell structure with mostly silica in the core and templates forming a shell. Nanoparticle size is found to increase with temperature and decrease with solution pH, in qualitative agreement with results from experiment and the previous lattice model study. The low-coordination model makes it possible to model porosity in the silica core of nanoparticles. We use this feature to investigate the extent of template penetration into the silica core, a level of nuance missing in experimental data on the core−shell model. We find that template penetration is rare for bulky templates. We discuss the implications of this result for understanding the role of these nanoparticles in the growth of MFI, especially in light of recent experiments on the long-time behavior of nanoparticle suspensions.

I. Introduction

Zeolites are an industrially important class of nanoporous crystalline silica materials,[1] whose self-assembly mechanism remains largely unknown. Revealing this mechanism is crucial for rational control of zeolite pore size and shape, and may allow targeted crystallite shapes of anisotropic zeolites.[2] The problem is complicated by the competition between silica polymerization and silica−template interactions, and also by structure at many length scales from silica oligomers, rings, and cages to nanoscale critical nuclei and beyond. Experimental progress has remained slow because critical nuclei likely fall into the nanoscale blindspot between characterization methods such as NMR and X-ray crystallography. Molecular modeling is thus poised to shed light on this problem.[3] However, the length scales involved require the development of clever models that capture the essential chemistry and physics of zeolite formation. In this article, we report progress on a lattice model of silica−template nanoparticles that appear in the early stages of the formation of silicalite-1 zeolite.

The clear-solution synthesis of silicalite-1 (pure silica form of zeolite ZSM-5) has been investigated extensively as a model system to study the mechanisms of self-assembly of zeolites.[4] Upon hydrolysis of tetraethylorthosilicate (TEOS) in aqueous solutions containing the template tetrapropylammonium (TPA) hydroxide, precursor silica nanoparticles form spontaneously and finally evolve to TPA−silicalite-1, with each zeolite pore occupied by a TPA cation. However, the precise structure of these nanoparticles and their role in zeolite formation remains unknown, with many hypotheses reported in the literature. Schoeman postulated that the nanoparticles are colloidally stable species that do not directly participate in the formation of silicalite-1 but instead depolymerize to provide silica oligomers for subsequent zeolite crystallization.[5] Van Santen and co-workers hypothesized that zeolites form by reaction-controlled integration of precursor nanoparticles at crystal surfaces.[6] Kirschhock et al. hypothesized that the nanoparticles are actually "nanoslabs" with MFI crystal structure, and that silicalite-1 forms by direct aggregation of these nanoslabs.[7] The last two hypotheses point to a mechanism involving direct assimilation of nanoparticles into the eventual zeolite crystals.

Recent experiments have since shed light on these issues. An in situ SAXS and SANS study by Fedeyko et al. found that the precursor nanoparticles are formed with a typical size of about 3−5 nm, with a core−shell structure of a silica-rich core surrounded by a TPA-rich shell, in both fresh and aged TPA−silica precursor solutions.[8] These particles were found to bear no evidence of silicalite-1 structure, and remained stable at room temperature for days.[8] They studied the spontaneous formation of silica nanoparticles in basic solutions of small tetraalkylammonium (TAA) cations tetramethyl- to tetrabutyl-ammonium, finding that nanoparticle core size decreases with pH, increases with temperature, and remains nearly independent of the composition of the TAA cation.

Davis et al.[9] and Kumar et al.[10] carried out room-temperature studies of dilute TPA−silica solutions, observing them for over a year. They studied the evolution of TPA−silica nanoparticles, finding that their size continued to increase until day 100 and then remained nearly constant, with no evidence silicalite-1 structure. After 220−245 days of aging, a second population of larger particles emerged, showing evidence of silicalite-1 structure. TEM images revealed the particles to be agglomerates of small crystals with domains comparable in size to those of the nanoparticles. It was concluded that nanoparticles actively participate in the nucleation and crystallization processes as building blocks. These studies suggest a synthesis process that occurs through formation and aggregation of the nanoparticles

---

* Authors for correspondence. E-mail: monson@ecs.umass.edu; auerbach@chem.umass.edu.
† Department of Chemical Engineering.
‡ Department of Chemistry.

followed by crystallization to MFI within the aggregates. What remains largely unknown is the process by which TPA cations redistribute from their shell domain to the nanopores of silicalite-1.

Jorge et al.[11] developed a lattice gas model to simulate silica−template nanoparticle formation. This model was inspired in part by previous work on surfactant systems[12] and on self-assembly in the formation of mesoporous silica materials.[13] The model involves a ternary mixture of coarse-grained particles, including neutral silicic acid, its deprotonated conjugate base, and cationic TPA "particles". Jorge et al. found that nanoparticles spontaneously form in canonical Monte Carlo simulations, exhibiting a core of neutral silica with anionic silica on the surface surrounded by a layer of TPA. Parallel tempering Monte Carlo[14,15] simulations showed that these nanoparticles are metastable species, equilibrating to a bulk solid phase which, in our model, is one large cluster sequestering all available silica. The model nanoparticles resist agglomeration because of the TPA coating, which is not a network-forming component in this system. Nanoparticle size was found to decrease with solution pH and increase with temperature, consistent with experimental observations.[8] Experimental evidence for metastability comes from the observation that between the initial rapid evolution of nanoparticles and the appearance of the aggregates, there is a period during which the size and number of nanoparticles remain largely unchanged.[9] Heating the model nanoparticles produces desorptive fluctuations of TPA species which expose nanoparticle surfaces to further growth, leading to equilibration of the nanoparticles around 150 °C to the bulk solid phase, in reasonable agreement with experiment. However, because of the 6-fold coordination in the simple-cubic lattice, the model bulk solid is nonporous, precluding the incorporation of TPA into the silica core. In order to study the redistribution of TPA as nanoparticles evolve toward zeolite critical nuclei, a new model is required that allows pore spaces in a silica network. The objective of this paper is thus to refine the lattice model to mimic the tetrahedral framework structure of silica, and to allow template penetration into the silica core.
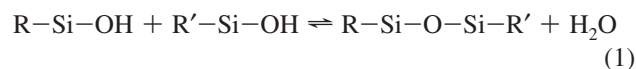
A four-coordinate tetrahedral network can be generated by using the body-centered cubic (bcc) lattice, which is equivalent to two interpenetrating tetrahedral lattices.[16] This feature has been used previously to model the network-forming substances such as water.[17−19] By imposing second-neighbor repulsions between silica units, the silica species are driven onto one of the two tetrahedral sublattices of the bcc structure. Refining the model of Jorge et al. in this way generates nanoparticles with four-coordinated tetrahedral networks possessing core−shell structures with silica in the core and template in the shell. More importantly, the unoccupied tetrahedral sublattice provides space (i.e., lattice sites) for template penetration. We find below that template penetration is a rare event; we discuss the implications of this result in light of the recent experimental work on the role of these nanoparticles in zeolite formation.

The outline of this paper is as follows. Section 2 presents the lattice model and its parameters. Section 3 describes the simulation techniques used. We present our results in section 4, and in section 5 we provide a summary of our results and conclusions.
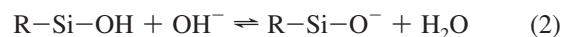
2. Model Description

The general features of our model closely follow those of Jorge et al.,[11] focusing on an aqueous solution containing tetraethyl orthosilicate (TEOS) and tetrapropylammonium hydroxide (TPAOH) at room temperature. Here we focus on the

implementation on a bcc lattice. At the isoelectric pH of silica (∼2), the condensation/hydrolysis reaction between neutral silica monomers (denoted by S_N) can be written in the generic form:

$$R-Si-OH + R'-Si-OH \rightleftharpoons R-Si-O-Si-R' + H_2O \tag{1}$$

The polymerization energy is modeled by an effective first-neighbor attractive interaction between silica units, with strength $\varepsilon_{S_N S_N}$. In our system, all the lattice sites are occupied by either solute or solvent; we consider the ethanol and water in the system as a single solvent with energy defined to be zero.[11] In order to generate the four-coordinated network that mimics the tetrahedral framework of silica, a second-neighbor repulsion was imposed between both neutral and ionized silica units. As discussed in the Introduction this has the effect of driving these species on to one of the diamond sublattices of the bcc lattice. This is the principal difference between the present model and that of Jorge et al.[11] All nonzero energies in this paper are scaled by $|\varepsilon_{S_N S_N}|$. The reduced temperature is defined as $T^* = k_B T / |\varepsilon_{S_N S_N}|$, where k_B is Boltzmann's constant.

Silicalite-1 is commonly synthesized under conditions of high water/silicon ratio and high pH where the following reaction also becomes important:

$$R-Si-OH + OH^- \rightleftharpoons R-Si-O^- + H_2O \tag{2}$$

To describe the polymerization process, we differentiate ionized monomers (denoted by S_I) from neutral monomers S_N. As shown below, if the S_I-S_N attraction is too weak, most ionized silica remains in solution; if too strong, an ordered solid phase arises with strictly alternating S_I and S_N, which is most likely an artifact of the model. For consistency with our previous work, we struck this balance with an S_I-S_N attraction of $-0.8|\varepsilon_{S_N S_N}|$.

We treat the interactions involving ionized silica as orientation-dependent: the magnitude of interactions varies as a given molecule approaches to the negatively charged oxygen or the neutral hydroxyl group. We assigned a pointer variable to each lattice site occupied by S_I to represent the anionic end of S_I, labeled as S_I^-. This variable "points" to one of the neighbors of that site, indicating the position of the negatively charged oxygen.[11] For example, at the first-neighbor level, the interaction between the pointer variable indicating the anionic end of S_I and neutral silica (denoted as $\varepsilon_{S_N S_I^-}$) is different from that between the neutral end group of ionized silica and neutral silica ($\varepsilon_{S_N S_I}$). The interaction $\varepsilon_{S_N S_I^-}$ is set to zero because such a condensation would produce a hydroxide group, which at high pH is extremely unlikely.

With a focus on modeling template penetration, we investigate below how the size dependence of templates influences penetration probability. We study "small" and "large" templates modeling TMA and TPA, respectively. The electrostatic attraction between TMA and S_I^- is a first-neighbor interaction. For the interactions involving TPA, we note that the diameter of the TPA cation is about 1.5 times that of the silica monomers.[20] This size effect is treated by adding a first-neighbor repulsion shell around each TPA unit. With a strong enough repulsion, all first-neighbor sites around each TPA remain unoccupied. For consistency with our previous study, we set this repulsion to $+5|\varepsilon_{S_N S_N}|$; the precise magnitude of this repulsion controls the extent of template penetration as discussed below. A second-neighbor repulsion between each pair of TPA cations is also

Lattice Model of Silica−Template Nanoparticles

J. Phys. Chem. C, Vol. 114, No. 34, 2010 **14395**

TABLE 1: Reduced First-Neighbor Interaction Parameters for the TMA Model

ε_{ij}^{FN}	S_I^-	S_I	S_N	TMA
S_I^-	0	0	0	−2
S_I	0	0	−0.8	0
S_N	0	−0.8	−1	0
TMA	−2	0	0	0

TABLE 2: Reduced Second-Neighbor Interaction Parameters for the TMA Model

ε_{ij}^{SN}	S_I^-	S_I	S_N	TMA
S_I^-	5	5	5	0
S_I	5	5	5	0
S_N	5	5	5	0
TMA	0	0	0	0

TABLE 3: Reduced First-Neighbor Interaction Parameters for the TPA Model

ε_{ij}^{FN}	S_I^-	S_I	S_N	TPA
S_I^-	0	0	0	5
S_I	0	0	−0.8	5
S_N	0	−0.8	−1	5
TPA	5	5	5	5

TABLE 4: Reduced Second-Neighbor Interaction Parameters for the TPA Model

ε_{ij}^{SN}	S_I^-	S_I	S_N	TPA
S_I^-	5	5	5	−2
S_I	5	5	5	5
S_N	5	5	5	5
TPA	−2	5	5	5

added. Because of the larger size of TPA, the electrostatic attraction between TPA and S_I^- must be extended to the second-neighbor level, which brings the pointer variable that represents the negatively charged oxygen in S_I^- to the second neighbors as well. As a result, we assign both first- and second-neighbor pointer variables, taking care that they both correspond to the same negatively charged oxygen.

We ignore S_N−TAA (either TMA or TPA) attractions because quantum chemical calculations have shown that these are comparable with TAA−water interactions,[21] which we also ignore for simplicity. For the first-/second-neighbor attraction between TMA/TPA and S_I^-, we set the attraction to $\varepsilon_{TAA-S_I^-} = -2|\varepsilon_{S_N S_N}|$ consistent with our previous work. As we show below, this attraction corresponds to a value of −6.6 kcal/mol based on the S_N−S_N energy obtained in section 4.1. This value of $\varepsilon_{TPA-S_I^-}$ is slightly larger than the free energy well depth of 4.7 kcal/mol computed for the interaction of cubic silicate polyion TMA^+ in aqueous solution.[22]

The Hamiltonian of the lattice model can be written as

$$H = \frac{1}{2} \sum_{i=0}^{3} \sum_{j=0}^{3} (N_{ij}^{FN} \varepsilon_{ij}^{FN} + N_{ij}^{SN} \varepsilon_{ij}^{SN}) \qquad (3)$$

where superscripts FN and SN denote first- and second-neighbor interactions. Indices 1, 2, and 3 refer to S_I, S_N, and TAA species, respectively, while the index 0 refers to interactions involving S_I^-. Tables 1 and 2 represent the reduced parameters for the TMA model, while Tables 3 and 4 summarize the reduced interaction parameters for TPA model. Following Jorge et al.[11] the TPA−TPA and TMA−TMA interaction parameters are

chosen to generate only size-exclusion, with the larger size of the TPA reflected in both first- and second-neighbor repulsions.

3. Simulation Methods

We use canonical ensemble (NVT) Monte Carlo (MC), grand canonical ensemble MC, and parallel tempering MC simulations[23,24] to investigate the properties and behavior of this bcc model. Most of the results presented in this paper were obtained from NVT MC simulations. Grand canonical MC was used to confirm that the canonical simulations of silica solubility are converged with respect to system size. Parallel tempering MC simulations were used to increase the probability that the system can cross large barriers between local minima of the free energy, and thereby locate equilibrium states in systems with the tendency to be trapped in metastable states. We use these simulations to provide evidence that the nanoparticles formed in our NVT simulations constitute a metastable state. Given that the nanoparticle states we find are metastable, it might be reasonable to ask whether the states are sensitive to the simulation path followed. As we are using a lattice model, the most obvious move to make would be short-range displacements so that the evolution of the system would follow Kawasaki-like dynamics.[25] We have found that the resulting dynamics is too slow for us to observe the self-assembly processes in these systems in a reasonable amount of computer time. Instead, as described below, we use larger scale moves so that the system follows Glauber-like dynamics.[25] We believe that this speeds up the kinetics without changing the mechanism of self-assembly or the nature of the metastable states formed in the system.

In the NVT MC simulations there are two types of MC moves implemented. The first kind of move is an occupancy swap between two species on different lattice sites. If an ionized silica is chosen, the value of its pointer variable stays the same during a swap. Since the concentration of template and silica are relatively low, most sites of the bcc lattice are unoccupied (sites occupied by solvent are treated as unoccupied because all the interactions involving solvent are set to zero). In order to avoid the inefficiency of attempted swaps between two solvent sites, we build an occupied site list. The first site is chosen randomly from that list, and the second site is chosen randomly from all the lattice sites of the system. The move is then accepted or rejected based on the usual Metropolis criterion.

The second kind of move is the rotation of a pointer variable for ionized silica monomers. This is implemented as follows. We randomly pick one site from the occupied site list and check the type of species on that site. If it is occupied by ionized silica, then the new pointer(s) is(are) assigned; otherwise that move is rejected. For the first-neighbor model, the new pointer is chosen randomly from eight possible values (eight first-neighbors). When it comes to the second-neighbor model, both first- and second-neighbor pointers are updated. The first-neighbor pointer is chosen randomly from 8 possible values, and the second-neighbor pointer is chosen consistent with the new first-neighbor pointer. After the new pointer(s) is(are) updated, the rotation is accepted or rejected according to the same Metropolis criterion.

Each NVT MC run was initiated from a random configuration in a cubic simulation box of length L bcc sites. The initial concentrations of S_I, S_N and TAA species were determined from experimental conditions.[11] The system was allowed to equilibrate for at least 3 million steps. A step is defined as N_{occ} attempted swaps plus N_{occ} pointer rotations, where N_{occ} is the number of occupied sites on the lattice. Cluster sizes were calculated using the Hoshen-Kopelman cluster-counting algorithm.[26] For the

core−shell structure calculation, we first labeled all the occupied lattice sites according to the Hoshen-Kopelman algorithm, calculated the center of mass of each nanoparticle, and histogrammed the core−shell structure of all nanoparticles. For the TPA model involving second-neighbor attractions, the Hoshen−Kopelman algorithm remains valid if we label TPA according to the second neighbor to which it is connected.

The parallel tempering MC simulations are implemented by simulating M replicas of the original system, each replica in the canonical ensemble but at a different temperature T_i. After a preset number of conventional MC steps in each replica, replica exchange is attempted by switching the configurations between adjacent replicas. We first select two adjacent replicas randomly and accept or reject on the basis of the probability:[23,24]

$$p = \min\left\{1, \exp\left[\left(\frac{1}{k_B T_j} - \frac{1}{k_B T_i}\right)(E_j - E_i)\right]\right\} \quad (4)$$

The lowest temperature is usually the physical temperature of interest, while the highest temperature must be sufficiently high so that no replicas become trapped in local energy minima. The number of replicas, how to select the temperature grids, and how frequently to employ replica exchange are presented in detail elsewhere.[11,14,15,27] Most of our parallel tempering simulations used 28 replicas with code run on a multiprocessor computer system, with the communications between processors handled by the Message Passing Interface library. The temperature grid was optimized through trial and error and the 28 reduced temperatures were: $T^* = 0.18, 0.1828, 0.1856, 0.1886, 0.1916, 0.1948, 0.1980, 0.2014, 0.2048, 0.2084, 0.2121, 0.2160, 0.2200, 0.2242, 0.2274, 0.2307, 0.2342, 0.2377, 0.2413, 0.2451, 0.2490, 0.2530, 0.2571, 0.2614, 0.2658, 0.2704, 0.2751, 0.28.$

4. Results and Discussion

4.1. Simulations for Model Parametrization. We begin by discussing the simulation studies that were used in estimating parameters for the model, as presented in section 3. We first calibrate the S_N-S_N interaction energy that mimics the condensation reaction of silica. To do this, we studied a system containing only neutral silica and solvent, comparing the canonical and grand canonical simulation results with experimental data on silica solubility to fit the energy scale of S_N-S_N attractions. These NVT MC simulations were initialized with a slab of close-packed silica in contact with pure solvent (i.e., vacancies), with periodic boundaries in the directions perpendicular to the slab surface. The system was then allowed to equilibrate at different reduced temperatures, and silica solubility was computed over the low-density region of space. Because the slab acts as a reservoir for a bcc lattice gas, these NVT MC simulations were compared with corresponding grand canonical MC simulations to confirm that the slab size is sufficiently large to act as a proper reservoir. Figure 1 shows the solubility of silica at various temperatures. The best fit of solubility yields a S_N-S_N attraction of $\varepsilon_{S_N S_N} = -3.3$ kcal/mol. The deviation between experimental solubility of amorphous silica[28] and our simulation results presumably comes from the various approximations in the lattice model. The fitted value of the S_N-S_N interaction agrees with the silica dimerization energy of -3.2 kcal/mol from ab initio calculations.[21] A temperature of 298 K thus corresponds to a reduced temperature of $T^* = 0.18$ in the lattice model.

Now we turn to the calibration of the S_N-S_I interaction. As discussed in the paper by Jorge et al.,[11] the S_N-S_I interaction is studied by simulating dilute solutions containing an equimolar
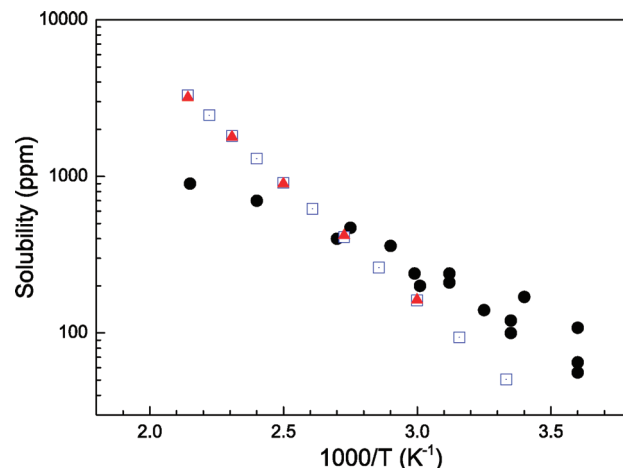

Figure 1. Solubility of amorphous silica at the isoelectric point as a function of temperature. The solid circles represent experimental data from Iler,[28] the solid triangles and open squares show the results of NVT and grand canonical Monte Carlo simulations, respectively. The best fit yields a S_N−S_N attraction of $\varepsilon_{S_N S_N} = -3.3$ kcal/mol.
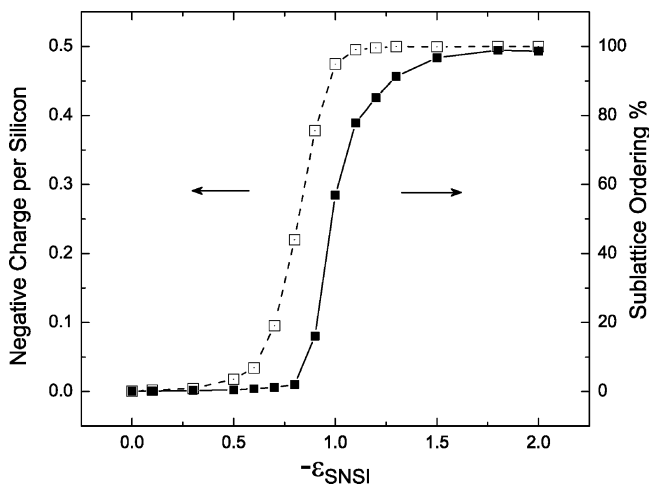

Figure 2. Simulation results for an equimolar solution containing neutral and ionized silica at room temperature ($T^* = 0.18$), using various values of the reduced interaction energy ε_{SNSI}. Open squares show the negative charge per silicon in the solid phase, and solid squares represent the degree of sublattice ordering in the solid phase.

mixture of S_N and S_I species. The parameter $\varepsilon_{S_N S_I}$ controls the partitioning of ionized silica between solution and solid phases, as well as the charge and structure of nanoparticles. When the S_N−S_I interaction is zero, most S_I is in solution and the negative charge per silicon is negligible. As the S_N−S_I interaction increases, more S_I is pulled into nanoparticles; the slope of this change is steep in the range of $\varepsilon_{S_N S_I}$ between -0.7 and -1.1. When $\varepsilon_{S_N S_I}$ is stronger than -1.2, almost all S_I is in the solid phase, and the negative charge per silicon reaches its limiting value of 0.5 (since the system we study is equimolar).

As the S_N−S_I interaction becomes strong, the nanoparticles appear as solids with alternating S_N and S_I (i.e., sublattice ordering). The degree of sublattice ordering is obtained by calculating the fraction of S_I with all S_N neighbors. As shown in Figure 2, when $\varepsilon_{S_N S_I}$ is less than -1.5, sublattice ordering becomes essentially complete. There are two criteria for choosing the S_N−S_I interaction: it must be large enough to allow the nanoparticles to be negatively charged, but not too large to force substantial sublattice ordering to occur. On the basis of these considerations we chose the bcc value of $\varepsilon_{S_N S_I} = -0.8$, consistent with our earlier work, although values in the range
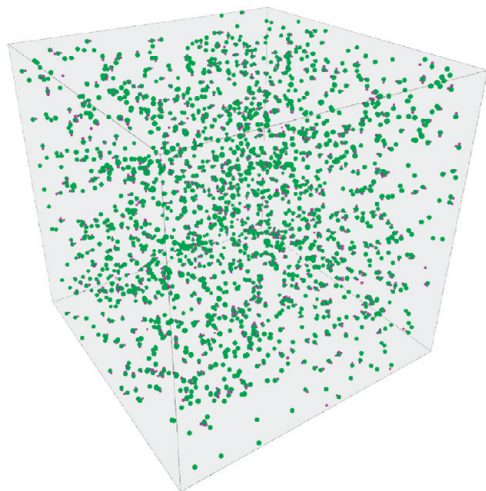
Figure 3. Snapshot of a configuration obtained during a simulation at $T^* = 0.18$, at composition C6. Red spheres are S_N molecules, purple spheres represent S_I molecules, and green spheres are TPA cations.

−0.7 to −0.9 give essentially the same results as is evident from Figure 2.

4.2. Formation and Stability of Nanoparticles. To study the formation and stability of nanoparticles we have investigated several compositions of the model corresponding to those used in recent experiments,[8,9] listed below as molar ratios:

composition C1, 40 SiO_2:9 TPAOH:9500 H_2O:160 ethanol
composition C2, 40 SiO_2:18 TPAOH:9500 H_2O:160 ethanol
composition C3, 40 SiO_2:5 TPAOH: 9500 H_2O:160 ethanol
composition C4, 20 SiO_2:9 TPAOH:9500 H_2O:80 ethanol
composition C5, 60 SiO_2:9 TPAOH:9500 H_2O:240 ethanol
composition C6, 5 SiO_2: 9 TPAOH: 9500 H_2O: 20 ethanol
composition C7, 40 SiO_2: 9 TMAOH: 9500 H_2O: 160 ethanol

For C6, most of silica is present in the form of dissolved monomeric species and no nanoparticles form, as shown in Figure 3.

When the mole fraction of S_N exceeds its solubility limit, silica nanoparticles form spontaneously[11] as shown in figure 4 at $T^* = 0.18$. The snapshots shown correspond to 5×10^4, 5×10^5, 2×10^6 and 6×10^6 MC steps. The visualizations in parts a−d of Figure 4 are consistent with growth by Ostwald ripening, because smaller nanoparticles can be seen to dissolve, adding their material to the larger nanoparticles. It is worth noting that global cluster moves are not included in our Monte Carlo move set. The clear solution synthesis is carried out at high pH and low concentrations, and the silica particles are negatively charged. The negative charges distributed on the surface of silica particles actually protect these particles from cluster−cluster aggregation through the electrostatic repulsions. The templates in our model have a repulsive interaction that would achieve the same effect. The average cluster size, reduced internal energy are plotted as a function of number of MC steps in Figure 5. There is a relatively rapid internal energy decrease at initial
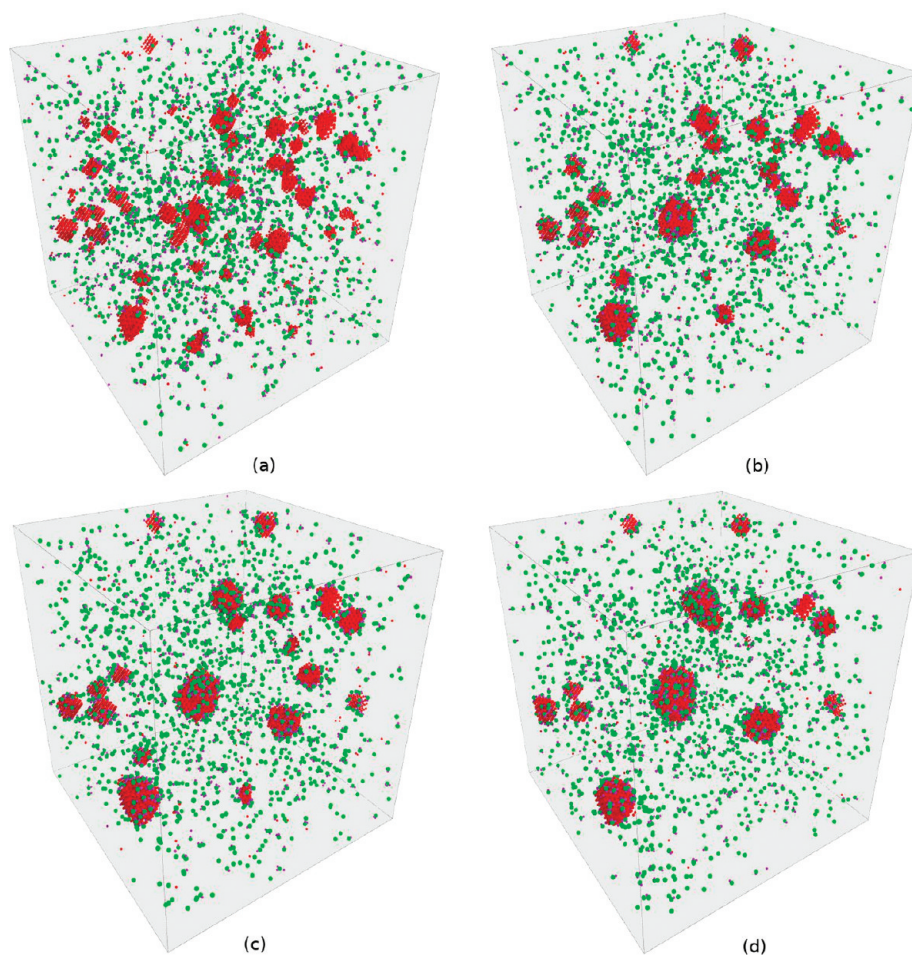

Figure 4. Evolution of silica−template nanoparticles over a single NVT MC run at $T^* = 0.18$ in composition C1. Snapshots are shown for: (a) 5×10^4, (b) 5×10^5, (c) 2×10^6, (d) 6×10^6 MC steps with lattice size $L = 100$. Red spheres are S_N molecules, purple spheres represent S_I molecules, and green spheres are TPA cations.
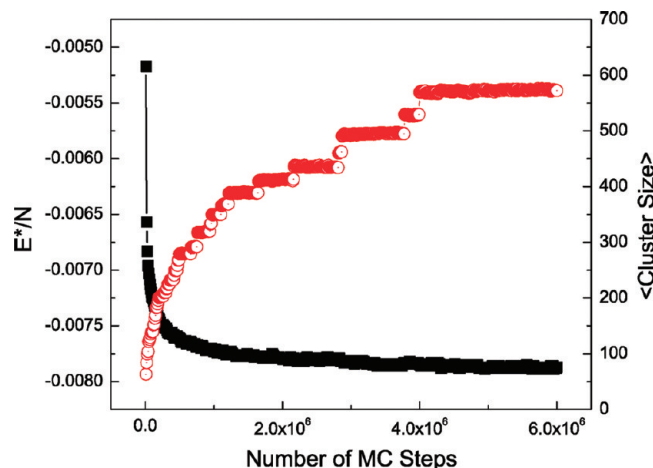
Figure 5. Evolution of a single NVT MC run at $T^* = 0.18$ of solution C1. Solid squares show the reduced internal energy per lattice site (left y axis), and open circles represent the average cluster size (right y axis).
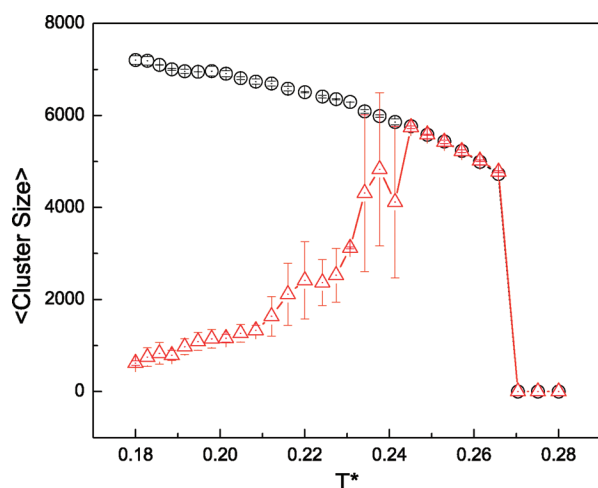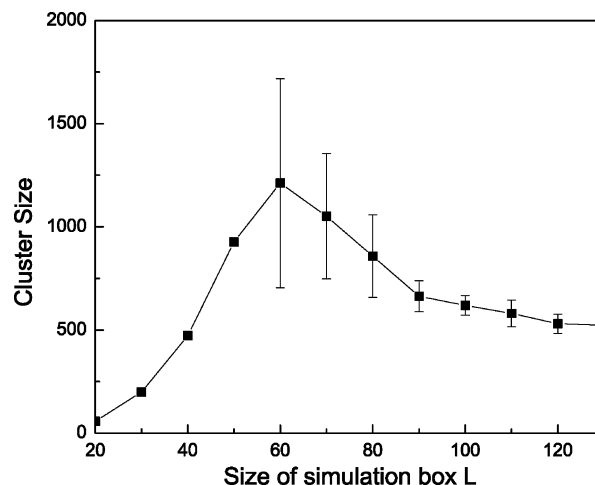

Figure 7. Average cluster size obtained from independent NVT simulations using different system sizes at composition C1. Cubic simulation boxes are used, and L is the cube edge length in bcc sites.

Figure 6. Average cluster size as a function of temperature with composition of C1. Open squares are obtained with parallel tempering, while triangles are results from NVT simulations, averaged over three independent simulations. Error bars represent one standard deviation.

stages because of the formation of small clusters. After about 4×10^6 MC steps, the average cluster size is seen to reach a plateau. We average the properties over a several statistically independent runs to converge the accumulation of statistics.

We have used parallel tempering MC simulations to investigate the thermodynamic stability of these nanoparticle systems. Figure 6 shows the average cluster size as a function of reduced temperature from both NVT and parallel tempering simulations; the results show qualitative agreement with our previous simple-cubic results.[11,29] At lower temperature there are two branches to the cluster size versus temperature behavior: one for the NVT MC simulations and one for the parallel tempering simulations. Below $T^* = 0.26$, all the parallel tempering simulations (open squares) produce a single large cluster (i.e., bulk solid phase), presumably representing the true equilibrium state of the system, and the average cluster size decreases with temperature. This decrease reflects the increasing solubility of silica with increasing temperature. When the temperature is high enough (above about $T^* = 0.26$), the bulk solid dissolves precipitously. In contrast to the parallel tempering simulations, the NVT Monte Carlo simulations produce nanoparticles that grow with increasing temperature. As with the simple-cubic model,[11] this can be

explained by increasing solubility of TPA, a capping agent, thereby allowing further particle growth. When heated to $T^* = 0.23 \pm 0.01$, the nanoparticles fluctuate wildly in size, allowing them to overcome the free energy barrier separating them from the bulk solid phase. Once the nanoparticles equilibrate fully to bulk solid, they remain in this state until heated to 0.26, at which point full dissolution occurs. Overall, these results corroborate the metastable nature of these nanoparticles by showing that this conclusion holds for more than one lattice.

We have investigated system size effects by computing mean cluster sizes for various simulation cell edge lengths $L = 20-130$ bcc sites. For each value of L, we have averaged over n_L statistically independent realizations. Values of n_L were chosen to keep the total simulated volume a constant, i.e., $n_L \times L^3$ was kept constant from one value of L to the next.[11] Figure 7 shows the average cluster size as a function of L. When $L < 80$, the average cluster size increases with L. This is because small systems always end up in a single cluster whose size grows with system size. For $L \geq 100$, multiple clusters are formed during all realizations, and the average cluster size approaches convergence. On the basis of these results we have used $L = 100$ in most of our simulations to balance convergence and computational cost.

4.3. Composition Distribution in Nanoparticles. We have calculated the distribution functions of silica and template within the nanoparticles shown in Figure 8a from NVT simulations. The distributions are normalized by setting the peak of each distribution function to unity. Fedeyko et al.[8] employed SANS and SAXS scattering methods to analyze the structure of silicate−TPA nanoparticles; their pair-distance-distribution function (PDDF) is reproduced in Figure 8b. In their experimental systems, X-rays are scattered primarily by silica whereas neutrons are scattered by both silica and TAA cations. In order to compare our simulation results with SANS data, we need to combine the silica and template distributions. However, no effective weighting function combining silica and template is available. To get a qualitative comparison, we used a linear combination of silica and template with equal weighting. Here we compare SAXS data with our silica distribution (black squares), and SANS data with our combined distribution profile (blue triangles). The nanoparticles obtained during NVT simulations possess a core−shell structure, with silica (black squares) in the core and TPA cations (red circles) in the shell, which is
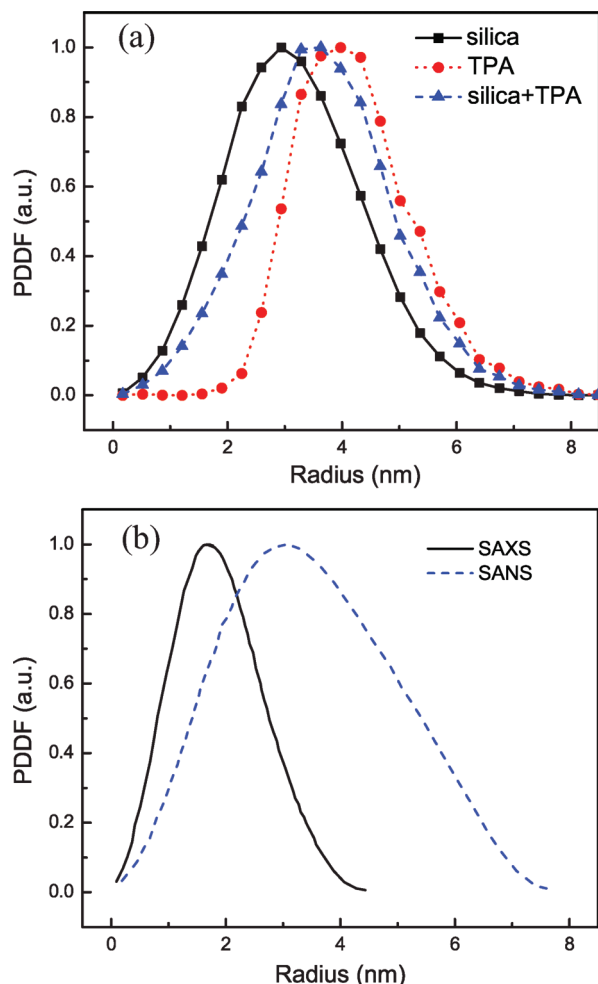
Lattice Model of Silica−Template Nanoparticles

J. Phys. Chem. C, Vol. 114, No. 34, 2010 **14399**

Figure 9. Radial distribution of nanoparticles evolution during MC run. Black squares, red circles, green up triangles, and blue down triangles correspond to 5×10^4, 5×10^5, 2×10^6, and 6×10^6 number of MC steps, respectively. Each distribution is a linear combination of silica and template distributions with equal weighting.

Figure 8. Silica−TPA nanoparticle structures at $T^* = 0.18$ with composition C1. (a) Radial distribution of silica, TPA and combined (silica + TPA) distributions from NVT simulation. Black squares and red circles represent the distribution of silica and TPA, respectively, x axis is the radius of nanoparticles in nm. Blue triangles are the linear combination of silica and template with a ratio of 1:1. (b) Experimental SANS and SAXS data from ref 8.

Figure 10. Snapshot of nanoparticles formed during NVT simulation at $T^* = 0.18$ with compositions C1. Red spheres are S_N molecules, purple spheres represent S_I molecules, and green spheres are TPA cations. (a) Snapshot of a single particle. The most compact structure formed using bcc lattice model with second neighbor repulsion is the β-cristobalite, as shown in this figure. Six-membered rings and channels are seen from this view. (b) Amplified view of rectangular region in (a). A TPA cation has penetrated inside the nanoparticles, as indicated by the black arrow.

consistent with experimental observations.[8] However, the experimental SANS pair-distance-distribution function (PDDF) is much broader than our combined radial distribution (blue triangles). This is probably because the experimental SANS PDDF not only counts molecules belonging to the nanoparticles but also includes ones in the electrostatic double layer surrounding the nanoparticles, while the simulated template distribution (see section 3) only considered templates directly adjacent to nanoparticles. The Debye length calculated from experimental conditions (temperature and ionic strength) yields 1.3 nm, partially accounting for this discrepancy between experiment and simulation.

Figure 9 shows the "combined" distribution function corresponding to different MC run lengths of 5×10^4, 5×10^5, 2×10^6 and 6×10^6 MC steps, respectively. These distribution profiles agree with snapshots shown in Figure 4. There is a relatively rapid increase in particle size during the first 5×10^4 steps, followed by slower particle growth after 5×10^4 steps, which agrees qualitatively with experimental observations.[9]

We now consider the penetration of TPA into the nanoparticles. Figure 10 shows a snapshot of nanoparticles formed during NVT simulation; six-membered rings and channels are seen from this view. More importantly, TPA cations (green
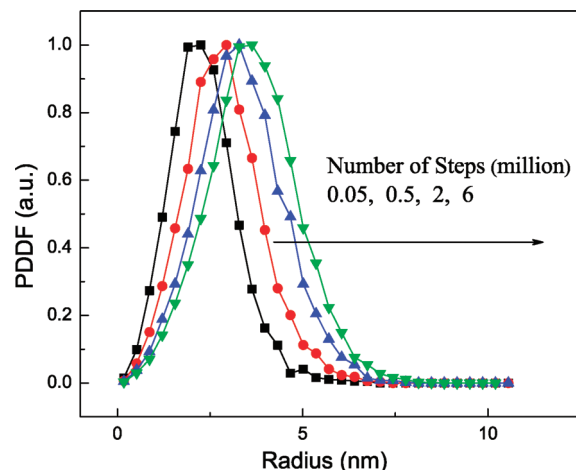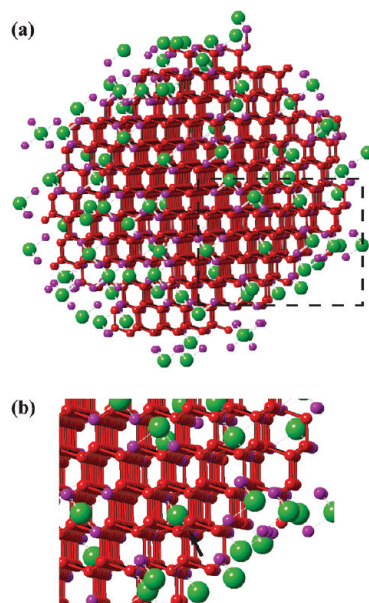
spheres) were observed inside the cores of nanoparticles. Penetration of TPA into the silica core in our model is rare because of the second-neighbor repulsion shell imposed around each TPA (see Table 4). To establish a baseline for TPA penetration, we note that the TPA/silicon ratio in TPA−silicalite-1 crystals is 4:96 or about 4.2%. In our simulations, the number of all TPAs associated with nanoparticles divided by the number of silica units in the nanoparticles is found to be 5.3%. This is quite comparable to the TPA loading in as-made silicalite-1. In contrast, the number of penetrating TPAs in nanoparticles divided by the number of silica in nanoparticles is about 0.2%, i.e., much less than in the zeolite. Nevertheless, the amount of penetrated TPAs is large enough to suggest that some TPA
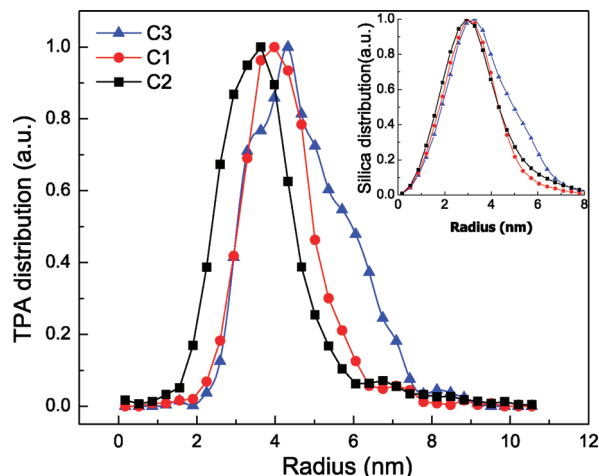
Figure 11. Radial distribution profiles of precursor nanoparticles at $T^* = 0.18$ with different TPAOH concentrations. Blue triangles, red circles, and black squares correspond to combined silica and TPA distribution in C3, C1, and C2 solutions, respectively.

Figure 12. "Combined" (Silica + TPA) radial distribution profiles of solutions $T^* = 0.18$ at different concentrations of silica, wherein black squares, red circles, and blue triangles correspond to compositions of C4, C1, and C5, respectively. Simulation distribution profiles are averaged over four independent runs at each composition.

Figure 13. Radial distribution of silica and TMA of nanoparticles formed during NVT simulation at C7. Solid squares represent the distribution of silica, and open circles show that of TMA. The triangles are equally weighted silica and template distributions.

cations reside in the silica core regions of precursor nanoparticles, a possibility that is not ruled out by the SANS and SAXS experiments.[8] We suggest that the rare incorporation of external TPA molecules within the interior of nanoparticles may explain the long induction period during clear-solution synthesis, and contribute to the decrease of their charge and long-term stability. Thus, we speculate that template penetration is key to silicalite nucleation.

The initial concentration of TPAOH controls both the concentration of TPA cations and solution pH. Experimental measurements have shown that increasing TPAOH concentration at constant silica concentration leads to smaller nanoparticles.[8] Figure 11 shows the distribution profiles of combined silica and TPA templates in precursor nanoparticles at $T^* = 0.18$ with different TPAOH concentrations. As the concentration of TPAOH increases from C3 (blue triangle) to C1 (red circle) to C2 (black square), while keeping the silica concentration constant, the sizes of the silica cores decrease slightly while the distribution profiles for TPA vary significantly. In particular, the C3 system with low TPA concentration shows tails in both core and shell distributions, suggesting there is not enough TPA to completely encapsulate the nanoparticles.

In Figure 12, we show "combined" (Silica + TPA) radial distribution profiles for different concentrations of silica while keeping the TPAOH concentration constant. As the concentration of silica is doubled (C1) and tripled (C5) compared to solution C4, nanoparticle size shifts only slightly to larger sizes, consistent with experimental observations that particle size is more sensitive to pH than to silica concentration (above a critical concentration).[8]

Experimental studies indicate that silica nanoparticles with similar structures also form spontaneously with other small TAA cations, such as tetramethylammonium (TMA), tetraethylammonium (TEA), and tetrabutylammonium (TBA).[8] To investigate how template size influences penetration into nanoparticle cores, we have studied nanoparticle formation with the TMA model of first-neighbor template-silica attractions. Figure 13 shows the radial distribution of silica and TMA of nanoparticles formed during NVT simulations. The nanoparticles formed with TMA have an average radius of 3.5 nm, estimated on the basis of a Si–O bond length of 0.16 nm, Si–O–Si angle of 150°, and the observed average radius of nanoparticles of 10 bcc lattice sites. The distributions of silica and combined
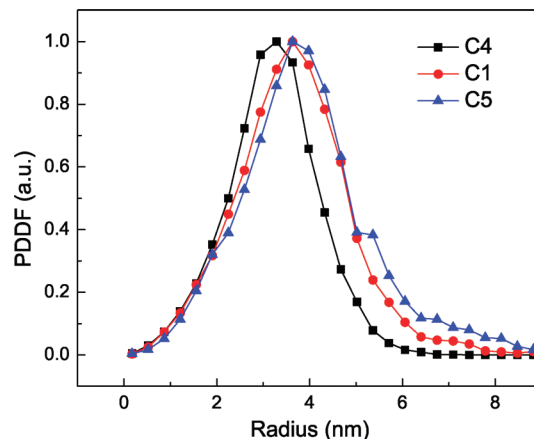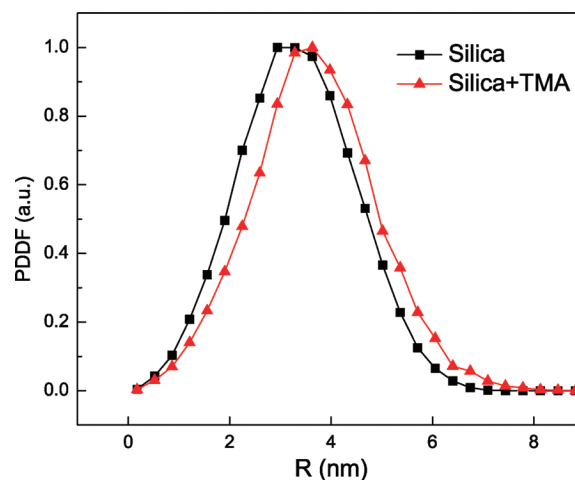
silica–TMA show similar behavior as the experimental X-ray and neutron scattering data for TMA nanoparticles.[30]

Fedeyko et al. interpreted their silica–TMA nanoparticle scattering data in light of core–shell structure.[30] However, our simulation results do not support this interpretation, considering that the width of our simulated "shell" is only a fraction of the size of TMA. As shown in Figure 14, a significant number of TMA cations are observed penetrating inside nanoparticle cores. We also observe that the size of silica–TMA nanoparticles is about the same as silica–TPA nanoparticles. In other words, the nanoparticle core size is found to be nearly independent of template size, in agreement with experimental observations.[8]

5. Conclusions

We have presented an extended version of the lattice model of Jorge et al. for studying the early-stage formation of nanoparticles during silicalite zeolite nucleation. By implementing the model on a bcc lattice and imposing a second-neighbor repulsion, we obtained precursor silica nanoparticles with a tetrahedral coordinated network and with remaining sites to act as pore spaces. We observed the spontaneous formation of silica–template nanoparticles under conditions comparable to
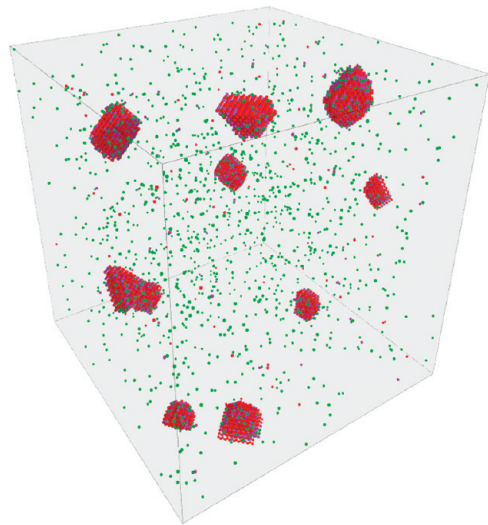
Lattice Model of Silica−Template Nanoparticles

J. Phys. Chem. C, Vol. 114, No. 34, 2010 **14401**

Figure 14. Silica and TMA nanoparticles formed during NVT MC run at $T^* = 0.18$ in C7 solution after 6×10^6 MC steps with lattice size $L = 100$. Red spheres are S_N molecules, purple spheres represent S_I molecules, and green spheres are TMA cations. Significant TMA penetration into nanoparticle cores is seen from these snapshots.

experiments. The nanoparticles were found to be metastable, equilibrating to bulk solid at high enough temperature. The metastability of these nanoparticles can be explained by their hierarchical structure: a core of mostly neutral silica, with ionic silica located mainly on the particle surface, surrounded by a layer of TPA cations. The TPA cations tend to adsorb to silica anions near the nanoparticle surface, thus providing a barrier protecting the nanoparticles from further addition of silica monomers.

Silica and template composition profiles were calculated to analyze the precise structures of nanoparticles. The nanoparticles were found to possess a structure consisting of a silica core and a template shell, consistent with experimental SANS and SAXS results. The size of simulated nanoparticles was found to increase with temperature and to decrease with solution pH (TPA concentration). Increasing the silica concentration at constant pH increased the number of nanoparticles and only slightly increased their size as well.

The most significant feature of the refined bcc lattice model is that templates can and do penetrate the interior of nanoparticles. Although in our simulated nanoparticles the template/silica ratio is comparable to that in as-made TPA−silicalite, the penetrating-template/silica ratio is 25 times smaller. We suggest that incorporation of the template into nanoparticles may play an important role during evolution from metastable nanoparticles to the nearly final state in the synthesis of silicalite-1 − with template molecules sitting in the intersections of zeolite. In future work, we will further develop such low-coordination models to investigate template penetration and nanoparticle structure along the path toward zeolite synthesis.

References and Notes

(1) Auerbach, S. M., Carrado, K. A., Dutta, P. K., Eds. *Handbook of Zeolite Science and Technology*; Dekker Inc.: New York:, 2003.

(2) Barton, T. J.; Bull, L. M.; Klemperer, W. G.; Loy, D. A.; McEnaney, B.; Misono, M.; Monson, P. A.; Pez, G.; Scherer, G. W.; Vartuli, J. C.; Yaghi, O. M. *Chem. Mater.* **1999**, *11*, 2633–2656.

(3) Auerbach, S. M.; Ford, M. H.; Monson, P. A. *Curr. Opin. Colloid Interface Sci.* **2005**, *10*, 220–225.

(4) Singh, R.; Dutta, P. K. In *Handbook of Zeolite Science and Technology.*; Auerbach, S. M., Carrado, K. A., Dutta, P. K., Eds.; Dekker Inc.: New York:, 2003.

(5) Schoeman, B. J. *Microporous Mesoporous Mater.* **1998**, *22*, 9–22.

(6) de Moor, P. P. E. A.; Beelen, T. P. M.; van Santen, R. A. *J. Phys. Chem. B* **1999**, *103*, 1639–1650.

(7) Kirschhock, C. E. A.; Ravishankar, R.; Jacobs, P. A.; Martens, J. A. *J. Phys. Chem. B* **1999**, *103*, 11021–11027.

(8) Fedeyko, J. M.; Rimer, J. D.; Lobo, R. F.; Vlachos, D. G. *J. Phys. Chem. B* **2004**, *108*, 12271–12275.

(9) Davis, T. M.; Drews, T. O.; Ramanan, H.; He, C.; Dong, J. S.; Schnablegger, H.; Katsoulakis, M. A.; Kokkoli, E.; McCormick, A. V.; Penn, R. L.; Tsapatsis, M. *Nat. Mater.* **2006**, *5*, 400–408.

(10) Kumar, S.; Wang, Z. P.; Penn, R. L.; Tsapatsis, M. *J. Am. Chem. Soc.* **2008**, *130*, 17284–17286.

(11) Jorge, M.; Auerbach, S. M.; Monson, P. A. *J. Am. Chem. Soc.* **2005**, *127*, 14388–14400.

(12) Larson, R. G. *J. Chem. Phys.* **1989**, *91*, 2479–2488.

(13) Siperstein, F. R.; Gubbins, K. E. *Langmuir* **2003**, *19*, 2049–2057.

(14) Hukushima, K.; Nemoto, K. *J. Phys. Soc. Jpn.* **1996**, *65*, 1604–1608.

(15) Kofke, D. A. *J. Chem. Phys.* **2002**, *117*, 6911–6914.

(16) Kittel, C. *Introduction to Solid State Physics*; Wiley: New York:, 1996.

(17) Bell, G. M.; Salt, D. W. *J. Chem. Soc., Faraday Trans. 2* **1976**, *72*, 76–86.

(18) Borick, S. S.; Debenedetti, P. G. *J. Phys. Chem.* **1993**, *97*, 6292–6303.

(19) Liu, J.-C.; Monson, P. A.; van Swol, F. *J. Phys. Chem. C* **2007**, *111*, 15976–15981.

(20) Zana, R.; Yeager, E. *J. Phys. Chem.* **1967**, *71*, 4241–4244.

(21) Catlow, C. R. A.; David, S. C.; Ben, S.; Lewis, D. W.; Pereira, J. C. G. In *Handbook of zeolite science and technology*; Auerbach, S. M., Carrado, K. A., Dutta, P. K., Eds.; Dekker Inc.: New York: 2003; pp 91–171.

(22) Caratzoulas, S.; Vlachos, D. G.; Tsapatsis, M. *J. Am. Chem. Soc.* **2006**, *128*, 16138–16147.

(23) Swendsen, R. H.; Wang, J. S. *Phys. Rev. Lett.* **1986**, *57*, 2607–2609.

(24) Earl, D. J.; Deem, M. W. *Phys. Chem. Chem. Phys.* **2005**, *7*, 3910–3916.

(25) Newman, M. E. J.; Barkema, G. T. *Monte Carlo Methods in Statistical Physics*; Clarendon Press, Oxford University Press: New York:, 1999.

(26) Hoshen, J.; Kopelman, R. *Phys. Rev. B* **1976**, *14*, 3438–3445.

(27) Yan, Q. L.; de Pablo, J. J. *J. Chem. Phys.* **1999**, *111*, 9509–9516.

(28) Iler, R. K. *The Chemistry of Silica: Solubility, Polymerization, Colloid and Surface Properties and Biochemistry*; Wiley: New York:, 1979.

(29) Jorge, M.; Auerbach, S. M.; Monson, P. A. *Mol. Phys.* **2006**, *104*, 3512–3522.

(30) Fedeyko, J. M.; Vlachos, D. G.; Lobo, R. F. *Langmuir* **2005**, *21*, 5197–5206.

JP1044207